NEURODEVELOPMENT

Human-specific *ARHGAP11B* increases size and folding of primate neocortex in the fetal marmoset

Michael Heide[1]*, Christiane Haffner[1], Ayako Murayama[2,3], Yoko Kurotaki[4], Haruka Shinohara[4], Hideyuki Okano[2,3], Erika Sasaki[4], Wieland B. Huttner[1]*

The neocortex has expanded during mammalian evolution. Overexpression studies in developing mouse and ferret neocortex have implicated the human-specific gene *ARHGAP11B* in neocortical expansion, but the relevance for primate evolution has been unclear. Here, we provide functional evidence that *ARHGAP11B* causes expansion of the primate neocortex. *ARHGAP11B* expressed in fetal neocortex of the common marmoset under control of the gene's own (human) promoter increased the numbers of basal radial glia progenitors in the marmoset outer subventricular zone, increased the numbers of upper-layer neurons, enlarged the neocortex, and induced its folding. Thus, the human-specific ARHGAP11B drives changes in development in the nonhuman primate marmoset that reflect the changes in evolution that characterize human neocortical development.

Evolutionary expansion of the human neocortex is linked to our cognitive abilities (*1*–*6*). The human-specific gene *ARHGAP11B* (*7*, *8*) is implicated in this neocortical expansion because it is expressed in the human progenitor cells giving rise to neocortical neurons, and when overexpressed in developing mouse and ferret neocortex, two evolutionarily distant mammals, can induce features associated with neocortical expansion (*9*, *10*). *ARHGAP11B* arose ≈5 million years ago by partial duplication of ubiquitous *ARHGAP11A*, which encodes a Rho-GAP exhibiting nuclear localization (*7*–*9*, *11*). However, because of a point mutation that presumably occurred after the partial gene duplication event and leads to a human-specific change in protein sequence, ARHGAP11B lacks Rho-GAP activity in vivo and is localized in mitochondria. This promotes the proliferation of basal progenitors, which are implicated in neocortical expansion through glutaminolysis (*11*, *12*). Here, we tested ARHGAP11B's relevance for neocortical expansion in a nonhuman primate by expressing *ARHGAP11B* under the control of its own (human) promoter in transgenic fetal marmosets.

To express human-specific *ARHGAP11B* (*7*, *8*) (fig. S1A) in the common marmoset, we constructed a lentiviral vector. In this functionally verified vector (fig. S1, B and C), an ≈2.7-kb human genomic segment containing the *ARHGAP11B* promoter drives expression of an enhanced green fluorescent protein (EGFP) reporter, followed by the complete ARHGAP11B protein-coding sequence. The two proteins become separate polypeptides after translation because of the presence of a T2A self-cleaving sequence (fig. S1B). This expression vector was used to generate pregnant marmosets carrying *ARHGAP11B*-transgenic fetuses by following a previously established protocol (*13*). This protocol involves microinjection into fertilized marmoset oocytes and transfer of in vitro–developed embryos into foster mothers 3 to 5 days after ovulation (with the day of transfer being defined as day 0 of pregnancy; fig. S1D and table S1).

We confined our analyses to marmoset fetuses because we anticipated that expression of this human-specific gene would affect neocortex development in this animal. In light of potential unforeseeable consequences with regard to postnatal brain function, we considered it a prerequisite—and mandatory from an ethical point of view—to first determine the effects of *ARHGAP11B* expression on the development of fetal marmoset neocortex. To this end, we collected fetuses after Caesarian section at day 101 of the ≈150-day gestation (fig. S1D), a stage when neocortical development shows both progenitor cell division and production of neurons (destined mostly to the upper layers) and which corresponds to fetal human neocortical development at ≈16 weeks after conception. Of the seven *EGFP*- plus *ARHGAP11B*-transgenic marmoset fetuses obtained (table S1), five expressed both EGFP and ARHGAP11B in fetal neocortex, whereas two expressed neither (Fig. 1). In the five transgenic fetuses exhibiting EGFP and ARHGAP11B expression in neocortex, we found three or four lentivirus integration events at random genomic positions

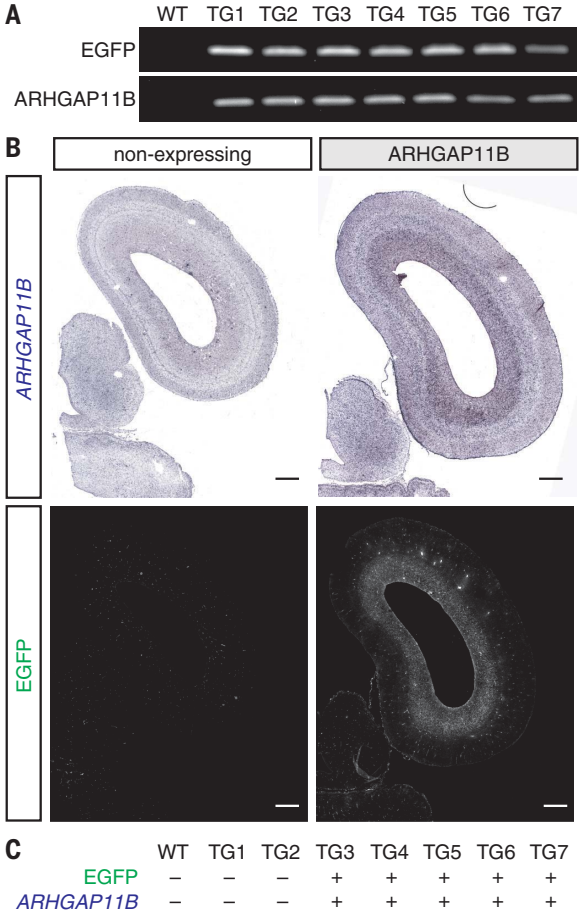

Fig. 1. *ARHGAP11B* and EGFP expression in *ARHGAP11B*-transgenic marmoset 101-day fetuses. Shown are the results of genomic PCR for *EGFP* and *ARHGAP11B* using somatic cells (**A**) and the absence (–) or presence (+) of EGFP protein and *ARHGAP11B* mRNA expression in neocortex (**B** and **C**) of one WT and seven *ARHGAP11B*-transgenic marmoset fetuses. (B) *ARHGAP11B* mRNA in situ hybridization (top) and EGFP immunohistochemistry (bottom) of *ARHGAP11B*-non-expressing (TG2) and *ARHGAP11B*-expressing (TG6) neocortex of marmoset fetuses. Scale bars, 500 μm.

[1]Max Planck Institute of Molecular Cell Biology and Genetics, 01307 Dresden, Germany. [2]Department of Physiology, Keio University School of Medicine, Tokyo 160-8582, Japan. [3]Laboratory for Marmoset Neural Architecture, RIKEN Center for Brain Science, Wako City, Saitama 351-0198, Japan. [4]Department of Marmoset Biology and Medicine, Central Institute for Experimental Animals, Kawasaki 210-0821, Japan.
*Corresponding author. Email: heide@mpi-cbg.de (M.H.); huttner@mpi-cbg.de (W.B.H.)

per animal (table S2). *ARHGAP11B* mRNA expression in the marmoset neocortical wall resembled that in fetal human neocortex, with similar intensity and occurring preferentially in the germinal zones [i.e., the ventricular zone (VZ), inner subventricular zone (iSVZ), and outer subventricular zone (oSVZ) (*14*)] (*9*, *15*), like EGFP, as revealed by in situ hybridization (fig. S1E) and reverse transcription quantitative polymerase chain reaction (PCR) (fig. S1F).

The *ARHGAP11B*-expressing marmoset neocortex was larger and its cortical plate (CP) thicker than that in normal marmoset neocortex (Figs. 1B and 2A and fig. S1E) and, in contrast to the smooth surface of the normal marmoset brain, exhibited surface folds (Fig. 2A). Quantification of fetal marmoset neocortex as a whole indicated no statistically significant difference in width but a significant increase in length of *ARHGAP11B*-expressing neocortex compared with wild-type (WT) and *ARHGAP11B*-non-expressing neocortex (Fig. 2B). To quantify cortical folding, we analyzed coronal sections of fetal marmoset neocortex along the rostrocaudal axis (Fig. 2C) to obtain the gyrification index (GI) (fig. S2A), which is the ratio of tracing the de facto length of the (unfolded or folded) cortical surface (Fig. 2E, green) over a hypothetical minimal length, i.e., smooth, tracing of the cortical surface (Fig. 2E, magenta) (*16*, *17*). Applying this tracing to the entire dorsoventral dimension of the coronal sections analyzed, WT and *ARHGAP11B*-non-expressing neocortex exhibited a GI of nearly 1.0 (Fig. 2C), consistent with the essentially unfolded, near-lissencephalic nature of the marmoset neocortex (*18*, *19*). The GI of *ARHGAP11B*-expressing neocortex increased rostrally (Fig. 2C) and reached nearly 1.1 when the tracing was confined to the portion of the cortical surface where gyrus-like structures emerged (Fig. 2D and fig. S2B). These structures did not arise by folding of a CP of equal thickness, but rather reflected local CP thickening (fig. S2, C to E), which in turn reflected a specific increase in upper-layer neurons as revealed by immunostaining for markers of specific neuron populations (fig. S2, D and F).

We then quantified CP thickness in WT, *ARHGAP11B*-non-expressing, and *ARHGAP11B*-expressing marmoset neocortex, taking into consideration only regions where no gyrus-like structures emerged in the *ARHGAP11B*-expressing neocortex. This revealed increased CP thickness for *ARHGAP11B*-expressing neocortex compared with WT and *ARHGAP11B*-non-expressing neocortex (Fig. 3, A and B, and figs. S3 and S4A).

To understand the basis of this increase in CP thickness, we quantified CP nuclei that were positive for Tbr1 and Ctip2, two markers of deep-layer neurons, and CP nuclei that were positive for Satb2 and Brn2, which are expressed by upper-layer neurons (*20*, *21*) (Fig. 3A and fig. S4B). We observed a nearly 40 and 50% increase in Satb2$^+$ neurons and Brn2$^+$ neurons, respectively, but not in Tbr1$^+$ and Ctip2$^+$ neurons, in the CP of *ARHGAP11B*-expressing marmoset neocortex compared with WT and *ARHGAP11B*-non-expressing neocortex (Fig. 3C and fig. S4, C and D).

Consistent with the developmental stage of our analyses (fig. S1D), we noted that a substantial proportion of the Satb2$^+$ and Brn2$^+$ neurons observed in the cortical wall were found in the subplate (fig. S5, A and B), consistent with these neurons migrating to the CP (*22*, *23*). Accordingly, the numbers specifically of Satb2$^+$ and Brn2$^+$ neurons in the subplate

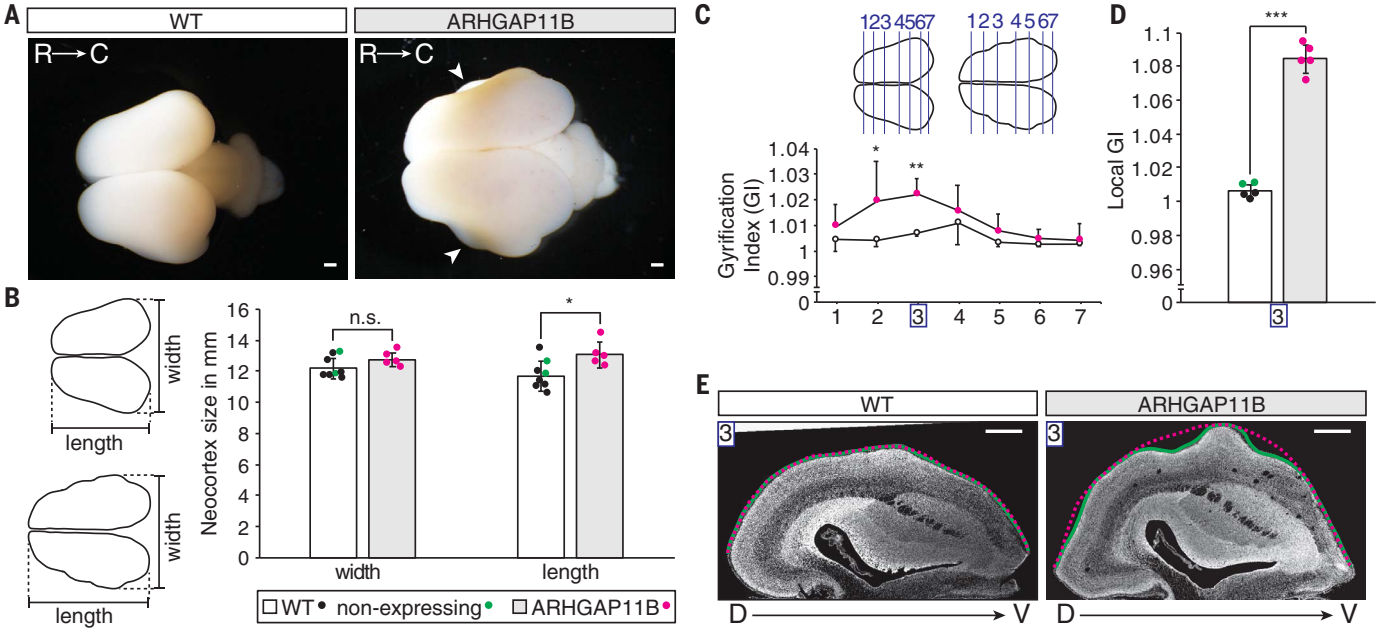

Fig. 2. Size and GI of WT and *ARHGAP11B*-non-expressing versus *ARHGAP11B*-expressing 101-day fetal marmoset neocortex. (**A**) WT brain and brain expressing *ARHGAP11B* in neocortex (TG3). Arrowheads indicate cortical folds. R, rostral; C, caudal. Scale bars, 1 mm. (**B**) Width and length (see diagrams) of six WT (black dots, white columns) plus two *ARHGAP11B*-non-expressing neocortices (green dots, white columns) versus five *ARHGAP11B*-expressing neocortices (magenta dots, gray columns). Data are shown as mean ± SD; n.s., not significant; *P < 0.05 (two-tailed t test). (**C**) GI [see (E) and fig. S2A] of three WT plus two *ARHGAP11B*-non-expressing neocortices (white circles) versus five *ARHGAP11B*-expressing neocortices (magenta circles) at seven positions along the rostrocaudal axis (see diagrams). Data are shown as mean ± SD; *P < 0.05; **P < 0.01 (one-tailed t test). (**D**) Local GI (see fig. S2B) of three WT neocortices (black dots, white column) plus two *ARHGAP11B*-non-expressing neocortices (green dots, white column) versus five *ARHGAP11B*-expressing neocortices (magenta dots, gray column). Data are shown as mean ± SD; ***P < 0.001 (two-tailed t test). (**E**) 4′,6-diamidino-2-phenylindole (DAPI)–stained coronal section of WT and *ARHGAP11B*-expressing (TG4) neocortex at position 3 [see (C)]. D, dorsal; V, ventral. Green line indicates the de facto length of the cortical surface; magenta line indicates the hypothetical minimal length of the cortical surface. Scale bars, 500 μm.

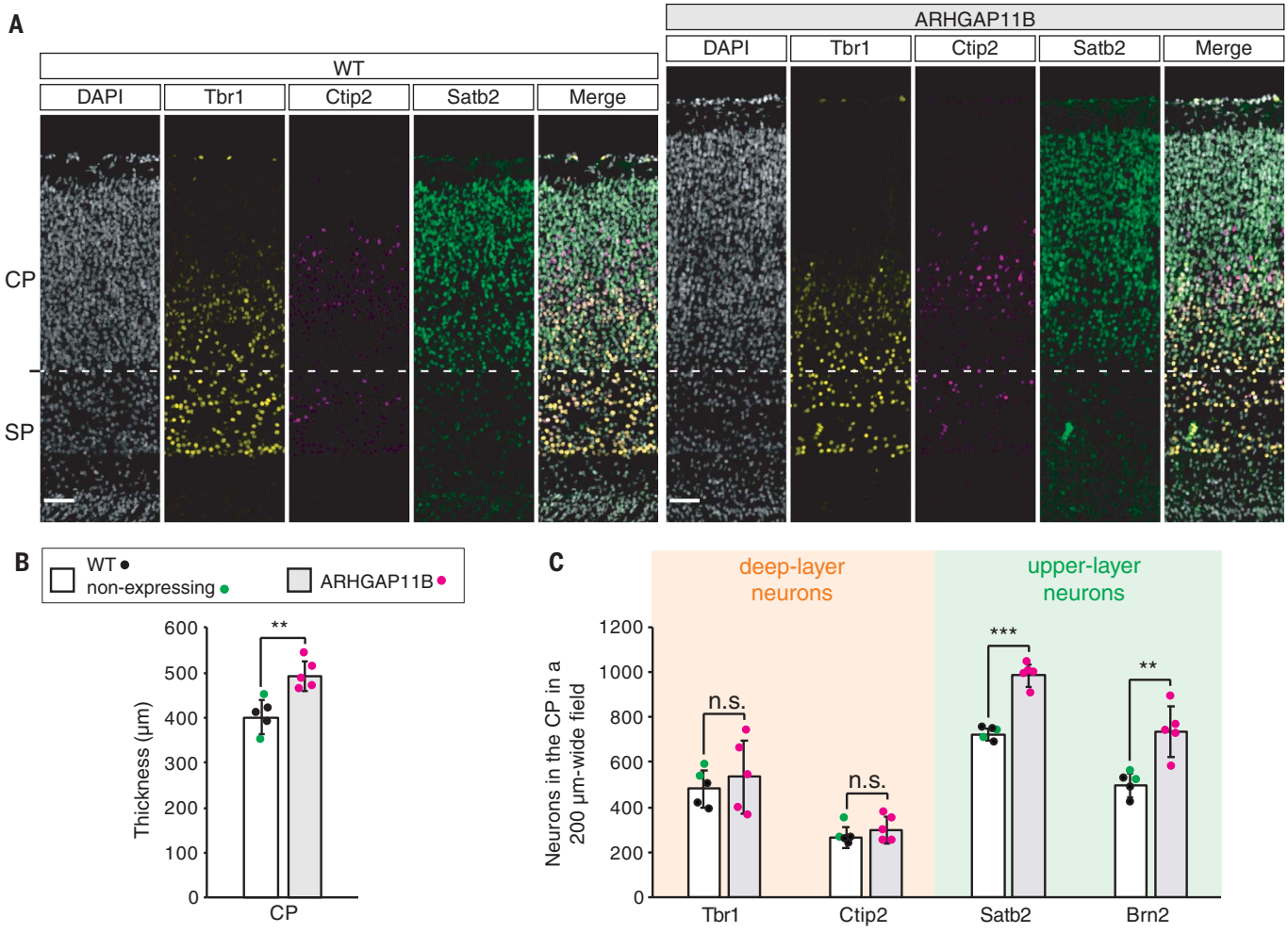

Fig. 3. *ARHGAP11B*-expressing 101-day fetal marmoset neocortex shows increased CP thickness and elevated numbers specifically of upper-layer neurons. (**A**) Triple immunofluorescence for Tbr1 (yellow), Ctip2 (magenta), and Satb2 (green) combined with DAPI staining (white), of WT (left) and an *ARHGAP11B*-expressing (TG3, right) neocortex (occipital lobe). Scale bars, 50 µm. (**B** and **C**) CP thickness (B) and Tbr1$^+$, Ctip2$^+$ Satb2$^+$, and Brn2$^+$ neuron number in CP in a 200-µm-wide field (C) of three WT neocortices (black dots, white columns) plus two *ARHGAP11B*-non-expressing neocortices (green dots, white columns) versus five *ARHGAP11B*-expressing neocortices (magenta dots, gray columns). For *ARHGAP11B*-expressing neocortex, quantification excluded gyrus. Data are shown as mean ± SD; $^{**}P < 0.01$; $^{***}P < 0.001$ (two-tailed *t* test).

were greater, but the subplate thickness was equal, for *ARHGAP11B*-expressing marmoset neocortex compared with WT and *ARHGAP11B*-non-expressing neocortex (fig. S5, C to F).

These data were consistent with an ongoing production of cortical neurons, mostly upper-layer neurons, at the developmental stage of our analyses (fig. S1D). We examined the germinal zones (VZ, iSVZ, and oSVZ) and progenitors therein for WT, *ARHGAP11B*-non-expressing, and *ARHGAP11B*-expressing marmoset neocortex (Fig. 4A). Analysis of the germinal zones showed increased oSVZ thickness for *ARHGAP11B*-expressing neocortex compared with WT and *ARHGAP11B*-non-expressing neocortex (Fig. 4B and fig. S7A). We observed an increase in mitotic basal progenitors that overall was ≈2-fold in the iSVZ and ≈3-fold in the oSVZ, but observed no difference in mitotic apical progenitors in the VZ (Fig. 4C and figs. S6 and S7, B and C).

At least half of the mitotic basal progenitors in the oSVZ of *ARHGAP11B*-expressing neocortex exhibited a basal process and thus were basal (or outer) radial glia (*24*–*27*), whereas this proportion was less (≤40%) for WT and *ARHGAP11B*-non-expressing neocortex (Fig. 4D and figs. S8, A to D), which is consistent with previous data (*28*, *29*). *ARHGAP11B* expression increased mitotic basal radial glia ≈3-fold (Fig. 4E and fig. S8E). A significant increase in basal radial glia caused by *ARHGAP11B* expression was also observed when these cells were quantified in interphase using the marker Hopx (*6*) (fig. S9). More than 99% of the mitotic basal radial glia in oSVZ were Sox2$^+$ (fig. S8F) and about half lacked expression of Tbr2 (Fig. 4, D and E, and fig. S8G). Therefore, the cells amplified upon *ARHGAP11B* expression in fetal marmoset neocortex exhibited a marker signature consistent with the identity of basal radial glia (*5*, *6*, *9*).

In this study, we examined physiologically relevant expression of human-specific *ARHGAP11B* (*7*, *8*) in the fetal neocortex of a nonhuman primate, the common marmoset, by using the human *ARHGAP11B* promoter, in contrast to previous studies using a strong constitutive promoter (*9*, *10*). This expression increased fetal neocortex size, CP thickness, upper-layer neurons, oSVZ size, and basal progenitors—including basal radial glia, the progenitor type that is thought to drive development of the mammalian neocortex (*2*–*6*, *14*, *30*). Our results suggest that the human-specific *ARHGAP11B* gene may have caused neocortex expansion in the course of human evolution.

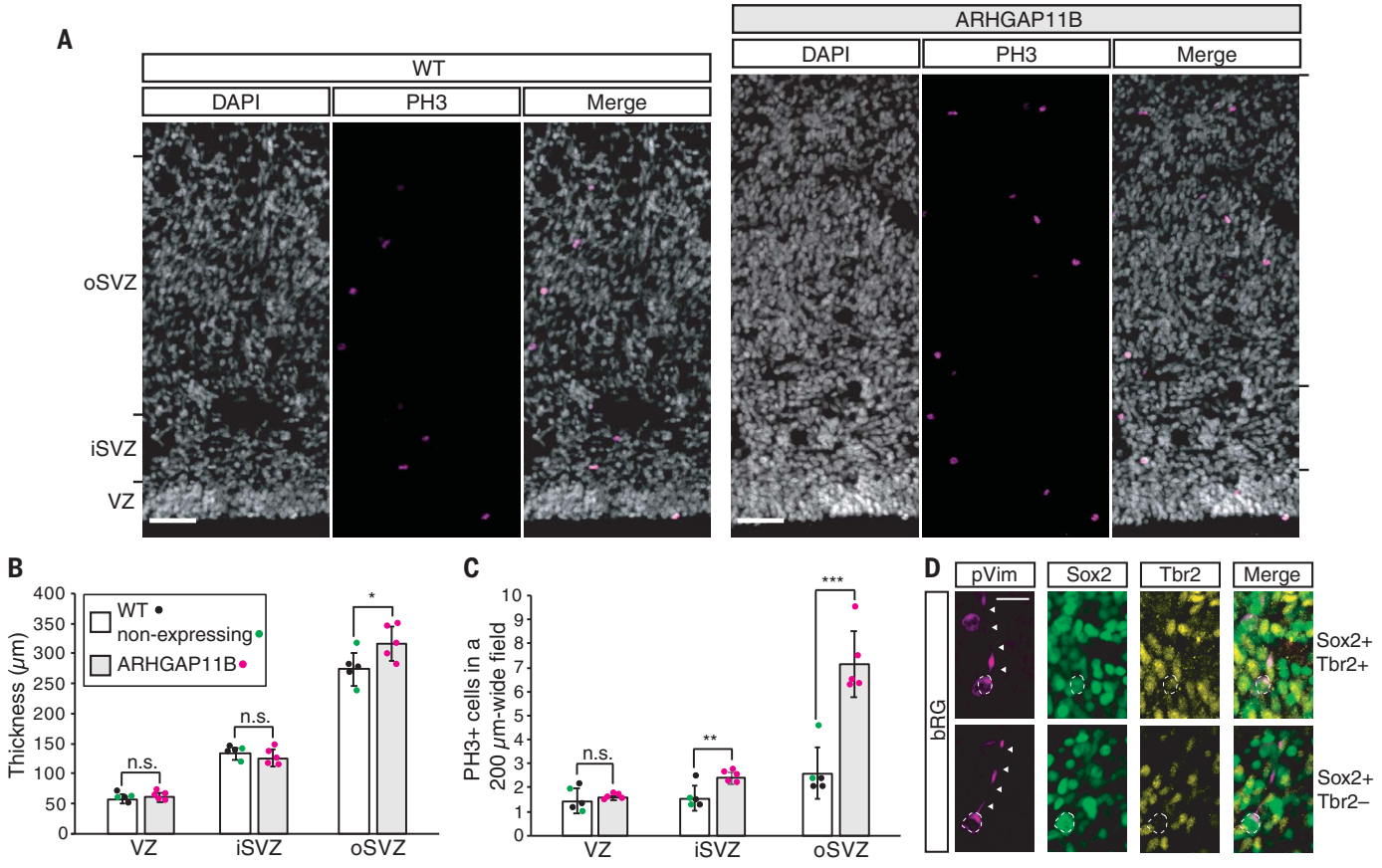

Fig. 4. *ARHGAP11B*-expressing 101-day fetal marmoset neocortex shows increased oSVZ thickness and elevated numbers of basal progenitors, notably basal radial glia. (**A**) Immunofluorescence for phosphohistone H3 (PH3, magenta), combined with DAPI staining (white), of WT (left) and *ARHGAP11B*-expressing (TG6, right) neocortex (occipital lobe). Scale bars, 50 μm. (**B** and **C**) Germinal zone thickness (B) and $PH3^+$ cell numbers in germinal zones in a 200-μm-wide field (C) of three WT neocortices (black dots, white columns) plus two *ARHGAP11B*-non-expressing neocortices (green dots, white columns) versus five *ARHGAP11B*-expressing neocortices (magenta dots, gray columns). Data are shown as mean ± SD; $*P < 0.05$; $**P < 0.01$; $***P < 0.001$ (two-tailed *t* test). (**D**) Triple immunofluorescence for phospho-vimentin (pVim, magenta), Sox2 (green), and Tbr2 (yellow) showing mitotic bRG in oSVZ of *ARHGAP11B*-expressing neocortex. Arrowheads indicate the basal processes. Top bRG shown is $Sox2^+$ $Tbr2^+$; bottom bRG is $Sox2^+$ $Tbr2^-$. Scale bars, 20 μm. (**E**) Numbers of total (left) and $Sox2^+$ $Tbr2^-$ (right) basal process–bearing $pVim^+$ cells in oSVZ in a 200-μm-wide field of four WT neocortices (black dots, white columns) plus one *ARHGAP11B*-non-expressing neocortex (green dot, white columns) versus three *ARHGAP11B*-expressing neocortices (magenta dots, gray columns). Data are shown as mean ± SD; $***P < 0.001$ (two-tailed *t* test).

REFERENCES AND NOTES

1. P. Rakic, *Nat. Rev. Neurosci.* **10**, 724–735 (2009).
2. J. H. Lui, D. V. Hansen, A. R. Kriegstein, *Cell* **146**, 18–36 (2011).
3. M. Florio, W. B. Huttner, *Development* **141**, 2182–2194 (2014).
4. C. Dehay, H. Kennedy, K. S. Kosik, *Neuron* **85**, 683–694 (2015).
5. Z. Molnár *et al.*, *J. Anat.* **235**, 432–451 (2019).
6. D. L. Silver *et al.*, in *The Neocortex*, W. Singer, T. J. Sejnowski, P. Rakic, Eds. (MIT Press, 2019), vol. 27 of Strüngmann Forum Reports, pp. 61–109.
7. P. H. Sudmant *et al.*, *Science* **330**, 641–646 (2010).
8. M. Y. Dennis *et al.*, *Nat. Ecol. Evol.* **1**, 0069 (2017).
9. M. Florio *et al.*, *Science* **347**, 1465–1470 (2015).
10. N. Kalebic *et al.*, *eLife* **7**, e41241 (2018).
11. T. Namba *et al.*, *Neuron* **105**, 867–881.e9 (2020).
12. M. Florio, T. Namba, S. Pääbo, M. Hiller, W. B. Huttner, *Sci. Adv.* **2**, e1601941 (2016).
13. E. Sasaki *et al.*, *Nature* **459**, 523–527 (2009).
14. I. H. Smart, C. Dehay, P. Giroud, M. Berland, H. Kennedy, *Cereb. Cortex* **12**, 37–53 (2002).
15. M. Florio *et al.*, *eLife* **7**, e32332 (2018).
16. K. Zilles, E. Armstrong, A. Schleicher, H. J. Kretschmann, *Anat. Embryol. (Berl.)* **179**, 173–179 (1988).
17. K. R. Long *et al.*, *Neuron* **99**, 702–719.e6 (2018).
18. K. Zilles, E. Armstrong, K. H. Moser, A. Schleicher, H. Stephan, *Brain Behav. Evol.* **34**, 143–150 (1989).
19. K. Sawada *et al.*, *Neuroscience* **257**, 158–174 (2014).
20. B. J. Molyneaux, P. Arlotta, J. R. Menezes, J. D. Macklis, *Nat. Rev. Neurosci.* **8**, 427–437 (2007).
21. S. Lodato, P. Arlotta, *Annu. Rev. Cell Dev. Biol.* **31**, 699–720 (2015).
22. K. Y. Kwan, N. Sestan, E. S. Anton, *Development* **139**, 1535–1546 (2012).
23. O. Britanova *et al.*, *Neuron* **57**, 378–392 (2008).
24. D. V. Hansen, J. H. Lui, P. R. Parker, A. R. Kriegstein, *Nature* **464**, 554–561 (2010).
25. S. A. Fietz *et al.*, *Nat. Neurosci.* **13**, 690–699 (2010).
26. I. Reillo, C. de Juan Romero, M. A. García-Cabezas, V. Borrell, *Cereb. Cortex* **21**, 1674–1694 (2011).
27. M. Betizeau *et al.*, *Neuron* **80**, 442–457 (2013).
28. I. Kelava *et al.*, *Cereb. Cortex* **22**, 469–481 (2012).
29. F. García-Moreno, N. A. Vasistha, N. Trevia, J. A. Bourne, Z. Molnár, *Cereb. Cortex* **22**, 482–492 (2012).
30. V. Borrell, M. Götz, *Curr. Opin. Neurobiol.* **27**, 39–46 (2014).

ACKNOWLEDGMENTS

We apologize to all researchers whose work could not be cited due to space limitations. We thank J. Okahara (Okano Lab in RIKEN CBS) for providing WT marmosets; J. Hata (Okano Lab in RIKEN CBS) for MR imaging of fetal marmoset brains; R. Behr (German Primate Center) for providing primary marmoset fibroblasts for initial construct and virus tests; D. Gerrelli, S. Lisgo, and their teams at the HDBR for the invaluable support from this resource; the Light Microscopy Facility, a Core Facility of the CMCB Technology Platform at TU Dresden, for scanning of cryosections; the Histology Facility of the CMCB Technology Platform at TU Dresden for cryosectioning; J. Peychl and his team of the Light Microscopy Facility at MPI-CBG for help with microscopy; G. Nadar of

the Scientific Computing Facility at MPI-CBG for help with data management; F. Friedrich and K. Margitudis for taking overview brain images; and T. Namba for providing the mouse monoclonal anti-ARHGAP11B IgG1 3758-A37-5. **Funding:** H.O. was supported by Brain/MINDS (JP20dm0207001) from AMED. E.S. was supported by the Strategic Research Program for Brain Science (JP17dm0107051) and Brain/MINDS (JP20dm0207065) from AMED. W.B.H. was supported by central funds of the Max Planck Society and by grants from the Deutsche Forschungsgemeinschaft (SFB 655, A2), the European Research Council (Advanced Grant 250197), and ERA-NET NEURON (MicroKin). **Author contributions:** Conceptualization: M.H., H.O., W.B.H.; Funding acquisition: H.O., E.S., W.B.H.; Investigation: M.H., C.H., A.M., Y.K., H.S.; Resources: H.O., E.S.; Writing – original draft: M.H., W.B.H.; Supervision: H.O., E.S., W.B.H.; Writing – review & editing: M.H., A.M., H.O., E.S., W.B.H. **Competing interests:** The authors declare no competing interests. H.O. and E.S. are inventors on the following patent applications: US 8592643 2013/11/26, Europe 2246423 2016/03/23, China ZL200880128383.3 (2014/11/26), Japan 5374389 (2013/9/27), Singapore 163739 (W02009/096101) 2013/09/30, and Korea 10-1588474 (2016/01/19) held by Keio University School of Medicine that covers "Method for introducing foreign gene into early embryo of primate animal" and "Method for production of transgenic primate animal comprising the introduction method." **Data and materials availability:** All data are available in the main text or the supplementary materials. Materials are available from M.H. or W.B.H. under a material transfer agreement and CITES permission.

SUPPLEMENTARY MATERIALS

science.sciencemag.org/content/369/6503/546/suppl/DC1
Materials and Methods
Figs. S1 to S9
Tables S1 to S4
Data S1
References (*31*–*33*)
MDAR Reproducibility Checklist

View/request a protocol for this paper from *Bio-protocol*.

10 February 2020; accepted 1 June 2020
Published online 18 June 2020
10.1126/science.abb2401

Science

Human-specific *ARHGAP11B* increases size and folding of primate neocortex in the fetal marmoset

Michael Heide, Christiane Haffner, Ayako Murayama, Yoko Kurotaki, Haruka Shinohara, Hideyuki Okano, Erika Sasaki and Wieland B. Huttner

Science **369** (6503), 546-550.
DOI: 10.1126/science.abb2401originally published online June 18, 2020

Neocortex in the fetal brain

Along the path of human evolution, gene duplication and divergence produced a protein, ARHGAP11B, that is found in humans but not nonhuman primates or other mammals. Heide *et al.* analyzed the effects of *ARHGAP11B* gene expression, under control of its own human-specific promoter, in the fetal marmoset (see the Perspective by Dehay and Kennedy). In the early weeks of fetal growth, the gene drove greater elaboration of neural progenitors and neocortex than is evident in the normal fetal marmoset. ARHGAP11B expression may be one cause of the more robust neocortex that characterizes the human brain.

Science, this issue p. 546; see also p. 506

Science (print ISSN 0036-8075; online ISSN 1095-9203) is published by the American Association for the Advancement of Science, 1200 New York Avenue NW, Washington, DC 20005. The title *Science* is a registered trademark of AAAS.